NASA

Technical Memorandum 80579

THE TIME-OF-FLIGHT SYSTEM ON THE GODDARD MEDIUM ENERGY GAMMA-RAY TELESCOPE

R. W. ROSS and J. R. CHESNEY

OCTOBER 1979

National Aeronautics and
Space Administration

Goddard Space Flight Center
Greenbelt, Maryland 20771

THE TIME-OF-FLIGHT SYSTEM ON THE GODDARD MEDIUM ENERGY GAMMA-RAY TELESCOPE

R.W. Ross and J.R. Chesney

NASA/Goddard Space Flight Center
Greenbelt, MD 20771

Abstract

A scintillation counter time-of-flight system has been incorporated into the Goddard 50 cm by 50 cm spark chamber gamma-ray telescope. This system, utilizing constant fraction timing and particle position compensation, digitizes up to 10 ns time differences to six bit accuracy in less than 500 ns. Event selection decisions, discriminating against upward-moving particles, are made prior to spark chamber triggering. The performance of this system during a November 1978 balloon flight is discussed.

Introduction

Since any instrument for gamma-ray detection intended for use in space operates in an environment of a large number of upward-moving gamma rays, some technique must be utilized to greatly reduce or eliminate the detrimental effect of this upward flux on detection efficiency. With a picture device such as a spark chamber there is little danger of misidentifying the upward-moving particle as a downward-moving gamma ray because of the unambiguous nature of the pair-production interaction. However, any time spent by the instrument in recording and transmitting unwanted data will reduce the live-time to some extent. Spurious counts could then, significantly reduce the instrument sensitivity by contributing excessive dead-time.

In previous instruments, an array of unidirectional Cerenkov counters was located at the bottom of the instrument as one element in the triggering telescope. The Cerenkov counters, blackened on the upper face, provided a fair rejection of the upward flux. However, for the Medium Energy Telescope discussed here and the High Energy Gamma-Ray Telescope reported elsewhere in these transactions[1], a time-of-flight technique has been adopted. By measuring the particle time-of-flight between two scintillators and rejecting times corresponding to upward-moving ones, the sensitivity of the instrument to this type of spurious event may be drastically reduced.

Description of the Instrument

The Medium Energy Gamma-Ray Telescope utilizes digitized wire grid spark chambers of similar design to previous balloon instruments[2] and the SAS-2 instrument.[3] The vertical spark chamber array consists of 20 wire grid modules, 50 cm by 50 cm inside dimension. Each module is constructed of glass-bonded-mica ceramic and wired with two orthogonal sets of 400 wires, one on each side of the frame. The x-y spark position is recorded by ferrite cores located on shelves at the edges of the module. As can be seen in Figure 1, the upper 16 spark chamber modules are closely stacked. These modules are interleaved with 25μm tantalum plates for gamma-ray/pair conversion. The four modules below the first scintillator plane are widely spaced to aid in identification of the separating electron-positron pair. These modules are separated by thin mylar light barriers only, to minimize any scattering or energy loss. The scintillators forming the time-of-flight telescopes are located just above and below the lower spark chamber stack and will be discussed in detail.

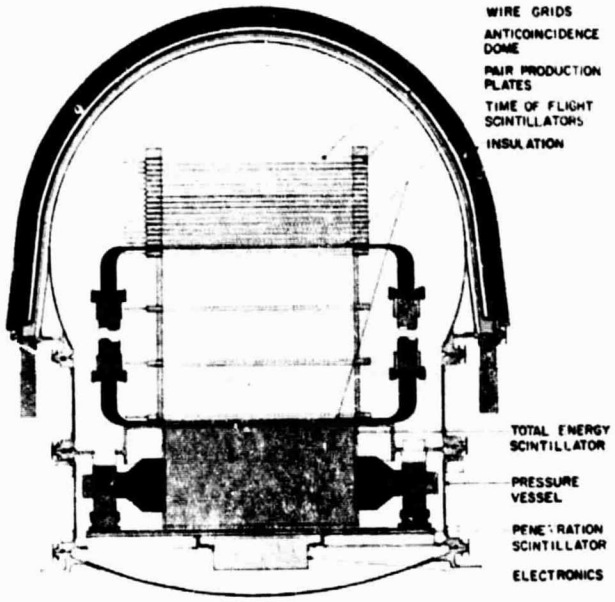

Figure 1. Cross section drawing of the Medium Energy Gamma-Ray Telescope.

The energy of the detected gamma ray is measured by the energy system in the lower section of the instrument. The heart of this system is a 50 cm by 50 cm by 25 cm block of plastic scintillator which is viewed by eight photomultipliers. The summed signal is pulse height analyzed to six bit resolution as a coarse measure of the energy of the produced pair. A 98 cm diameter plastic scintillator located below records penetrations of the energy scintillator to flag events where the charged particles did not deposit their total energy in the large scintillator. The upper portion of the instrument is surrounded by a 1.2 m diameter dome of plastic scintillator. This scintillator is used in anticoincidence with the other scintillator elements to veto incident charged particle penetrations.

The Time-of-Flight System

Overall Description

The upper and lower scintillation counters for the time-of-flight system are composed of three side-by-side strips of pilot B plastic scintillator measuring 50 cm by 16 cm by 6.3 mm thick. These scintillator strips are viewed at each end through adiabatic and isochronous plexiglas light guides by RCA 8575 photomultipliers. Since the entire upper chamber of the instrument is filled with Ne-He spark chamber gas,

the photomultipliers, resistor voltage dividers, and high voltage power supplies are enclosed in individual pressure-tight containers.

A block diagram of the instrument time-of-flight electronics is shown in Figure 2. The fast signals from each photomultiplier anode are routed to a slow coincidence discriminator module and bridged to the constant fraction discriminators where the timing signal is derived. Discriminator signals from each end of the scintillator are averaged by the time compensation circuit, and a single time-coincidence strobe is generated from each of the three strips. The time compensator signals act as Start and Stop for a dual-ramp time digitizer. The digital time-of-flight data are compared to a command entered threshold value for the up/down decision, and are also stored in an on-board memory. The time-of-flight data from each event meeting all the spark chamber trigger criteria are telemetered along with the "picture" data. The accumulated spectrum in the on-board memory is dumped via telemetry on a periodic basis independent of the spark chamber operation.

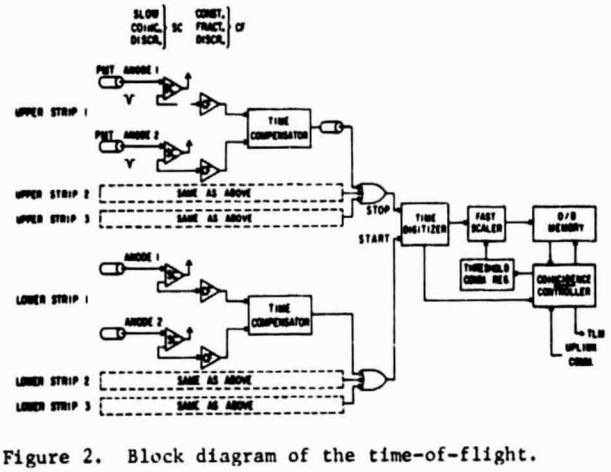

Figure 2. Block diagram of the time-of-flight.

Constant Fraction Discriminating

The timing signals are derived from the photomultiplier signals by an integrated circuit constant fraction of pulse height discriminator. This implemention of a well known technique[4] utilizes Motorola MC 1651 dual I.C. comparators as the fast switching elements. While the inherent switching speed of this ECL device is not as great as for a charge storage diode or tunnel diode, in this application this is of minor significance; however, the stability and rugged nature of the device is of overriding importance.

In the circuit of Figure 3, the I.C. 1b acts as a cross-over detector with the cross-over point adjustable by the variable resistor as shown. The input signal is attenuated to give a 0.2 fraction and applied to the non-inverting input. The unattenuated signal is delayed by a 3 ns length of semi-rigid microcoax and applied to the other input. I.C. 1a is used as a leading edge trigger to arm the AND gate I.C. 2a. The other half of I.C. 2 is used as a unity gain amplifier to facilitate inspection of the cross-over setting.

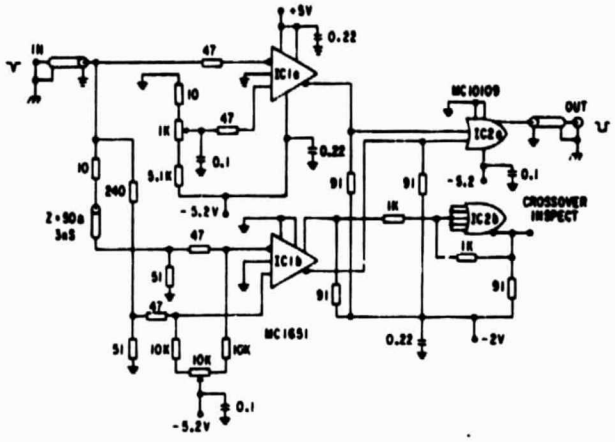

Figure 3. Schematic of the constant fraction discriminator.

Time Compensator

On this instrument the main axis dimension of the timing scintillators (50 cm) is on the same order as their separation (45 cm), so if some form of compensation were not used, the variation in the position of traversal of the scintillator by the particle would totally destroy the up/down timing resolution. By using the light signal from each end of these long scintillators it is possible to compensate for this variation. There are two techniques that are used for travel time compensation: the technique of linear addition of time-to-amplitude converter outputs[5], and the technique of the time averager.[6] The simplest implementation for this application uses the latter technique.

The schematic shown in Figure 4 represents the method of time compensation used for this instrument. The differential pairs Q1 and Q4 receive the standardized ECL signals from the constant fraction discriminators connected to the photomultipliers on opposite ends of a scintillator strip. I.C. 3b is a gate connected to generate the ECL reference voltage of -1.3v. Differential pairs Q2 and Q3 each launch 0.5 volt

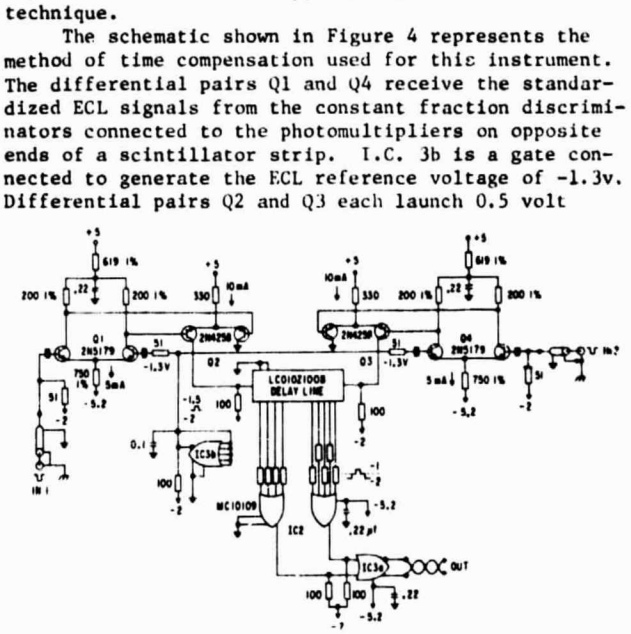

Figure 4. Schematic of the time compensator.

pulses into the 10 ns delay line. The combination of I.C. 2 and I.C. 3a form a logical OR with a threshold of -1.3v whose inputs are connected to the delay line taps. At the time the signals from each end of the delay line overlap and add, exceeding the -1.3v reference, an output signal is generated. This time is essentially independent of the position where the particle penetrates the scintillator.

Time Digitizer

The signals from the time compensators, which represent an average time-of-occurrence in the upper and lower scintillation counter strips, are transmitted via twisted pair cable to the time digitizer shown in Figure 5. The differential signals originating from the three upper and three lower scintillators are converted to single-ended by ECL line receivers and logically OR'd to be applied to the Start and Stop flip-flops (I.C. 1a,b). Prior to the occurrence of an event the conversion capacitor C is maintained at the reference voltage V_R by the differential amplifier-regulator made up of Q5, Q6, and Q7. On arrival of a Start pulse, the regulator is released and the pull-down current source Q8 begins to decrease the voltage across the capacitor. A Stop signal terminates the run-down by turning off Q8 and the run-up begins from current source Q9. The ratio of run-down to run-up current is the stretching factor of the circuit. The current sources are biased by zener diodes operated at near-zero temperature coefficient. The diode-connected transistors compensate the V_{be} variation of the current source transistors and should be in good thermal contact for best results. The capacitor voltage is sensed by the circuits of I.C. 4, (used here as a comparator) and a time gate is generated. It is initiated by the Stop pulse and lasts until the voltage across the capacitor returns to V_R. This time gate is applied to the delay line gated oscillator (I.C. 6) which generates a 175 Mhz train of pulses, digitizing the run-up time of the conversion capacitor. This pulse train is routed to a high speed ECL scaler in the digital section where this digitized time-of-flight is processed.

Supervisory logic functions, such as requiring valid Start before Stop, resetting the system whenever the time difference overranges, and holding when the digital data system is busy, are included on the digitizer board and shown in the schematic.

Digital Data System

This section will deal with the time-of-flight digital subsystem and how it interacts with the overall experiment event handling electronics. The on-board event handling system consists of a number of subsystems which perform the various tasks of time-of-flight measurement, pulse height analysis, command decoding and coincidence determination. The time-of-flight subsystem encodes the particle time-of-flight, generates an enable signal if a preset threshold condition is met, and accumulates the time spectra in on-board memory. The pulse height analyzer digitizes the signal amplitude from the energy scintillator, generates an enable signal if the pulse height exceeds the preset threshold, and accumulates the pulse height spectra in on-board memory. The command decoding and coincidence electronics form the telescope coincidence logic, subject to enabling signals from the time-of-flight, pulse height analyzer, anticoincidence, and ground commands. The instrument may be commanded into various spark chamber trigger modes; which may logically include or exclude the time-of-flight result, the pulse height value, the penetration counter flag, or the anticoincidence. The on-board storage conditions may be commanded independently. For instance, the spark chamber may be triggered on neutral events only, while a histogram of charged particle data is being accumulated.

The entire event handling system in under the control of an AMD2911 microprogram sequencer. The control program is contained in a 64 by 32 bit bipolar PROM. The controller handles transfer of data and control signals between the various subsystems, the control of on-board histogram memory, and the

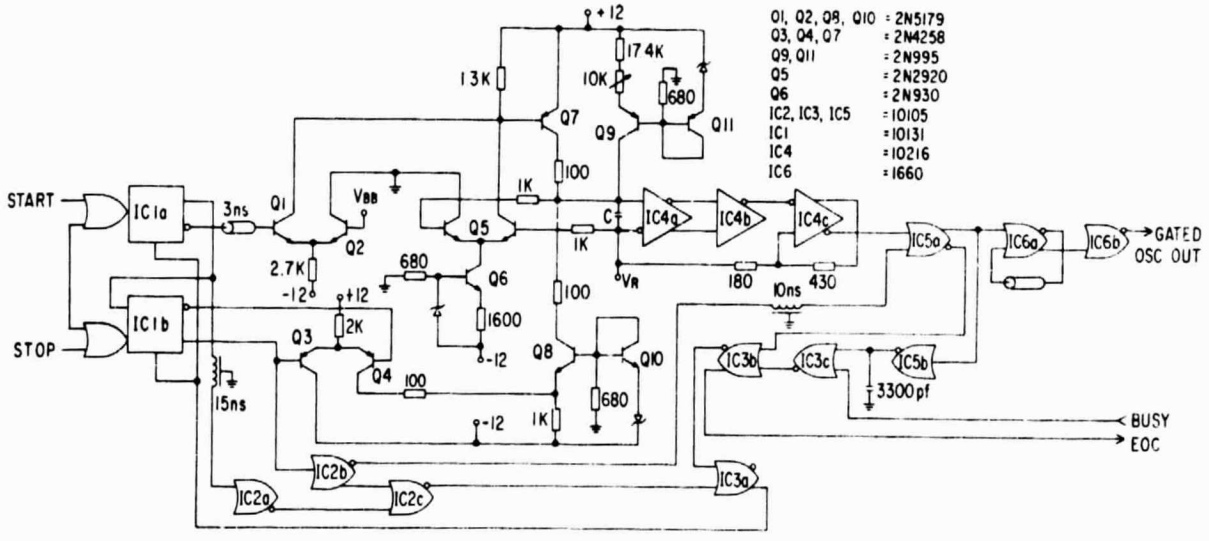

Figure 5. A simplified schematic of the time digitizer. ECL pull-down resistors and bypass capacitors are not shown.

retreival and transmission of event and histogram data to the experiment telemetry formatter.

A simplified block diagram of the event handling system as it relates to the time-of-flight is seen in Figure 6. The high frequency burst from the time digitizer gated oscillator is counted by a six bit ECL scaler. The translated time-of-flight data is parallel-loaded into the output T^{2}L shift register by the End-of-Conversion (EOC) pulse from the digitizer. The EOC pulse is also used to notify the coincidence subsystem that a TOF Event (TOFE) has occurred. The six bits of time-of-flight data are compared to the value held in the command register. A value less than this preset threshold causes a Time-of-Flight-Good (TOFG) enable to be sent to coincidence.

The accumulation of the time-of-flight histogram is controlled by the control/sequencer. The occurrence of a Read-Increment-Write (RIW) flag from coincidence causes the controller to increment the address determined by the value in the output shift register. The histogram memory is organized as a 6 channel by 64K count array. The RIW cycle time is about 3μsec. For events where a spark chamber trigger is generated the RIW sequence is held until the noise from the spark chamber has subsided.

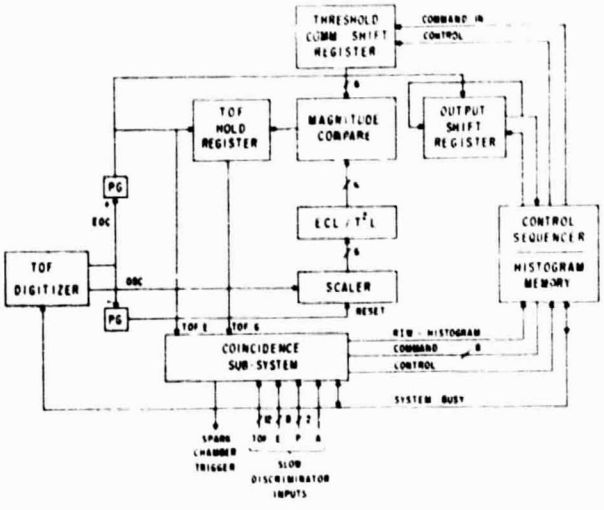

Figure 6. Block diagram of the time-of-flight digital data system.

System Performance

Laboratory Test

The constant fraction discriminators were tested for function and time response versus input amplitude characteristics prior to being integrated into the instrument. In order that the input pulse characteristic be representative of the actual application, a photomultiplier, scintillator, and small ^{241}Am α-source were used as the test pulse generator. A laboratory time-to-amplitude converter and multichannel analyzer were used to measure the performance. Typically, the circuits had less than 50 ps of time-walk for an input amplitude varied from -300 mV to -3 volts, a range representative of the instrument signals.

The timing characteristics of this instrument can be influenced by electronic broadening as well as the size and placement of the scintillators. In order to determine the relative contributions to the timing uncertainty a measurement was made of the inherent resolution of the instrument electronic system. The test technique was the γ-γ coincidence. Two small plastic scintillators were each viewed by an 8575 photomultiplier. A ^{60}Co source was placed between the scintillators, irradiating each with one of the coincident gammas. Prototype instrument discriminators and time digitizer were used for the fast timing, with the digital time-of-flight value being stored in a multichannel analyzer memory. Laboratory discriminators were used to gate the electronics to select the signal amplitudes to be analyzed. With an energy threshold slightly below the Compton edge, a resolution of about 320 ps FWHM was obtained.

The signals from the six individual scintillators are processed by a single time digitizer; the particular acceptance geometry determined by the coincidence electronics. It is necessary to balance the individual telescope delays to obtain best resolution. This was done using the spectra obtained from ground level cosmic rays. The photomultiplier high voltage supplies were set to give roughly constant signal levels and the constant fraction discriminators individually adjusted for walk compensation. Interconnecting cables were then trimmed in length so the timing peak from each of the three telescopes coincided. A plot of the response of the overall instrument time-of-flight system to ground level cosmic rays is shown in Figure 7. The instrument was operated for equal time in the normal and in the inverted position to obtain the "upward" and "downward" peaks. The width of the high-channel peak is 1.1 ns FWHM. The low-channel peak is slightly broadened, apparently due to observed counts from low level (about one count per second) natural radioactivity in the tantalum pair production plates above the time-of-flight scintillators.

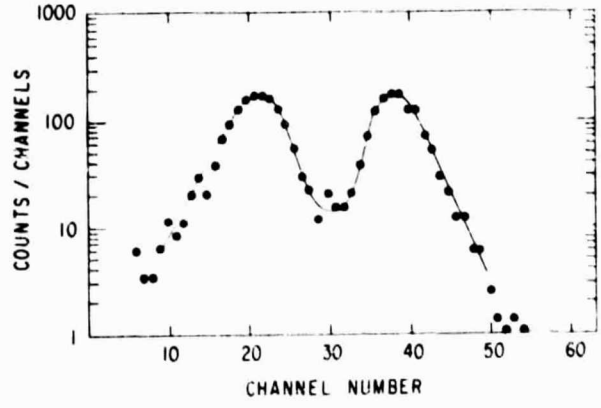

Figure 7. Preflight test results with the instrument upright (lower peak) and inverted (upper peak). The conversion factor was 160ps/channel.

Test Flight

On November 18, 1979 the Gamma-Ray Telescope was flown on a 1.2x10^5 m^3 balloon from Palestine, Texas. The purpose of this flight was both to test the instrumentation and to afford an opportunity to operate the instrument with various trigger modes to determine the optimum configuration for subsequent scientific flights. The balloon reached a pressure-altitude of 9 mbar, and the instrument performed well for the duration of the flight. Figure 8 is plot of two time-of-flight histogram dumps taken at float altitude. One set of data was taken with the anticoincidence electronics active, selecting neutral events, and the other with the anticoincidence off, selecting both charged and

neutral events. The peaks corresponding to upward and downward moving particles are clearly resolved for both the neutral and charged particles. However, these spectra are broadened considerably as compared to the ground level results. The distribution due primarily to charged particles has a width of about 1.5 ns, while the neutral events gave a greater time spread of 1.9 ns FWHM. Since the ground level data in Figure 7 were taken during a preflight checkout, it is presumed that his broadening is not caused by any instrument malfunction but is the result of background from multiparticle events and complex particle interactions in the instrument. Clearly, interactions in the walls of the spark chamber between the scintillator planes could generate simultaneous upward and downward-moving particles, broadening the peaks toward zero time. Additionally, for good gamma rays, the opening angle of the pair event can lead to an error in the time measurement.[7] The time compensator will generate a time-of-occurrence signal which is early by an amount proportional to the separation of the pair. Depending on exactly how the pair intersects the upper and lower scintillators, this can cause broadening toward either greater or lesser times.

Although the data deviate somewhat from Gaussian, an approximate fit was made to the distribution of neutral events. It was then possible to calculate the approximate number of events from the "upward-moving" peak which were greater than the trigger threshold at zero time. The result of 0.1 counts/second from the tail of the "upward-moving" curve implies less then 3 percent instrument dead-time, a small contribution to the overall measured dead-time of 75 percent at 9 mbar.

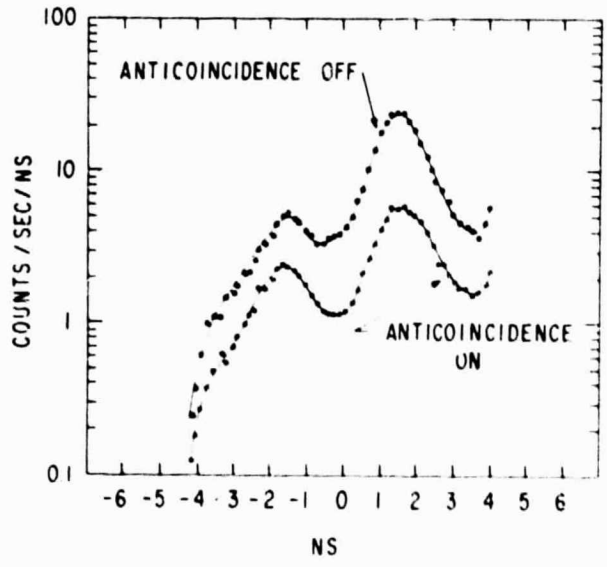

Figure 8. Time-of-flight spectra taken at 9 mbar during the test flight. Positive times represent the downward component.

Conclusions

In general, the performance of the time-of-flight electronic system during the test flight was as expected from laboratory evaluation. The timing characteristics as observed from several histogram dumps throughout the flight remained quite stable. The 500 ns delay for the time analysis caused no apparent deterioration in the spark chamber performance, nor did the spark chamber interfere with the time-of-flight histogram data collection. The timing resolution observed at float altitude was broader then anticipated apparently due to effects from multiparticle background, but the effect on instrument live-time appeared to be minimal.

A scientific flight with this instrument was attempted in Alice Springs, Australia on April 8, 1979 but did not succeed due to balloon failure. Another flight will be attempted in the near future.

Acknowledgements

The authors gratefully acknowledge many enlightening discussions and assistance in the interpretation of the test flight results from Drs. D. Bertsch and D. Knitten. We also wish to thank V.P. Cegan, W. Daniels, M. Mooring, and A. Smith for expert technical assistance during assembly and testing of the instrument.

References

1. F.B. Hughes, R. Hotstadet, A. Johannsen, J. Kolte, D.J. Bertsch, W.J. Chatekshank, C.H. Ehrmann, C.F. Fichtel, R.C. Hartman, D.A. Knitten, R.W. Ross, D.J. Thompson, K. Pinkau, H. Rothermel, M. Sommer, H. Mayer-Hasselwander, A. Favale, F. Schmeid, IEEE Transactions of Nuclear Science Symposium, October 17-19, 1979.

2. R.W. Ross, C. H. Ehrmann, C.F. Fichtel, D.A. Knitten, and H.B. Ogelman, IEEE Trans. Nucl. Sci., 16, No. 1 (1969) 304.

3. S.M. Derdeyn, C.H. Ehrmann, C.F. Fichtel, D.J. Knitten, and R. W. Ross, Nucl. Inst. and Meth., 95, (1971) 557.

4. M.R. Maier, P. Sperr, Nucl. Inst. and Meth., 87 (1970) 13.

5. G. Charpak, L. Dick, and L. Feuvrais, Nucl. Inst. and Meth., 15 (1962) 323.

6. J. Faust, R.S. Larsen, Nucl. Inst. and Meth., 116 (1974) 365.

7. H. Rothermel, IEEE Trans. Nucl. Sci., 24, No. 1 (1977) 801.